

Open source workflow for multispectral imaging based on artificial neural networks

This paper presents a workflow based on open source software for multispectral imaging specifically designed for analysis of works of art. Our workflow allows to capture radiometrically and colorimetrically accurate images, requiring only common photography equipment and a set of two optical filters. The input data is machine-processed using artificial neural networks to obtain interpretation-ready multispectral images. We provide the entire software package under the general public license.

Keywords: machine learning, multispectral imaging, works of art, image processing, open source

1. INTRODUCTION

Multispectral imaging (MSI) is a process of visualizing imaged objects in multiple spectral bands even outside the visible range of the electromagnetic spectrum (1). These bands can be selected by band-pass filters on either the detector or illumination source (2). Using a set of single-band filters, one can obtain useful results (3). Such implementation is, however, very time-consuming as images need to be captured as many times as many filters are used. An alternative strategy is to reduce the number of filters to only a few with distinct spectral transmittances across the entire imaged spectral range. The signal obtained through these filters together with the RGB channels defined by the Bayer mask on the detector can be numerically processed to estimate reflectivity in individual spectral bands (4). Whatever strategy is chosen, MSI allows extracting additional information about the imaged object namely at wavelengths inaccessible to the human eye. That is why it has found its practical usage in cultural heritage analysis by art historians (5; 6; 7).

Although MSI methods do not replace the capability of spectroscopic methods in general (8) or chemical analyses (9), MSI has the advantage of being a non-invasive and affordable method for analyzing important works of art (10) without the necessity of taking samples and thus without damaging the artwork as invasive methods usually do. Using MSI, we can map and identify historical pigments (11), retouches, and underpaintings, which cannot be normally observed because it is beyond the capabilities of the human eye (12). It does not always allow to distinguish between all possible pigments, because they are mixed and overlapped in multiple layers, but it is successful for those, which present particular behavior in the imaged spectral range (most commonly from ultraviolet to infrared parts of the electromagnetic spectrum). The possibility of imaging underpaintings depends on the upper layer of the painting (whether the layer absorbs, reflects, or transmits infrared radiation) and on the base layer, which can also absorb or reflect infrared radiation. It is also of a significant benefit to having the artwork digitized, because cracks in the lay-

ers of the painting and retouches are inimitable and thanks to that, historians of art can pass judgment for example on its authenticity, i.e. at what time the artwork was created, who created it and whether the artwork is original or fake (13).

The main purpose of this paper is to report on a workflow for imaging of works of art using a specially modified digital single-lens reflex camera and a set of optical filters. Machine learning (artificial neural networks, ANNs) is applied to process the obtained images for further usage in cultural heritage analysis. In the second section, the imaging workflow and the setup for imaging are introduced. The subsequent software processing is described step by step in the third section. Finally, the whole process is demonstrated on an example work of art (The Death of Sophonisba by an unknown artist) and the results are discussed in the last section. All software developed within the scope of this paper is available for download as the digital supplement (14).

2. IMAGING WORKFLOW SETUP AND IMAGE CAPTURE

2.1 Scene preparation

Acquisition of radiometrically or colorimetrically accurate images requires a well-defined imaging setup and adherence to the following procedure. Preferably, the imaged object should be carefully removed from its frame if possible. Illumination sources are deployed homogeneously as depicted in Figure 1, typically under 45 degrees with respect to the object's plane and it should be checked that the illumination does not cast shadows or cause specular reflections on the imaged object at least from the camera's perspective. Using a power meter with a set of optical filters one can verify that the illumination contains all required spectral bands. If a combination of several types of light sources is needed to cover the required spectral width, one also needs to check that the imaged object is covered spectrally homogeneously. There are several types of illumination sources. For instance, incandescent light bulbs are used to provide infrared illumination, because their emission peak is situated at 1300 nm. Light

panels with white and UV light tubes or LEDs provide visible and ultraviolet illumination. Attention should be paid to the white light source color rendering index (15).

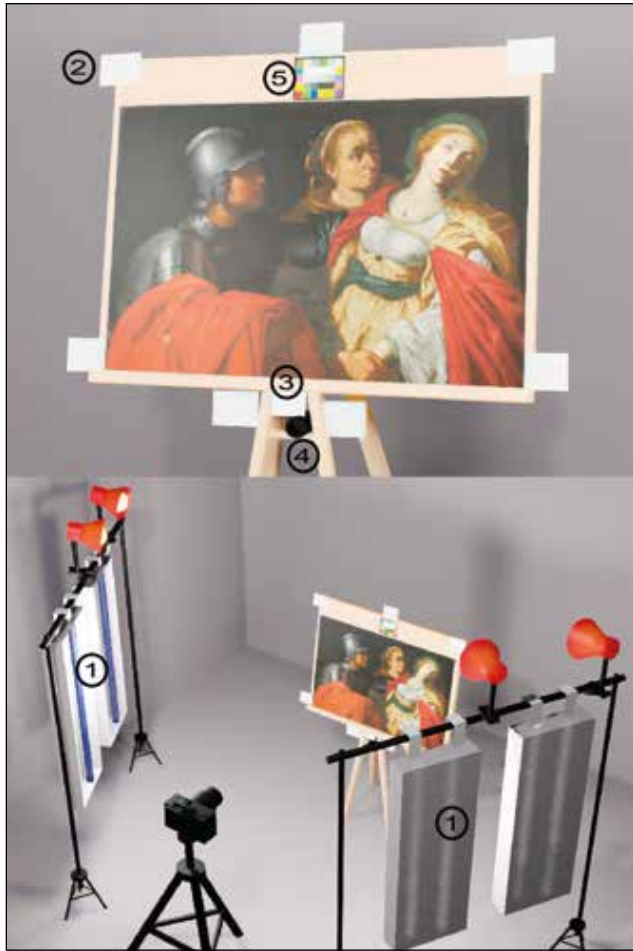


Figure 1: 3D model of the scene preparation. Note the layout of illumination sources (1) and installation of calibrating equipment such as the surrounding white cards (2), white standard (3), black hole (4) and colorchecker (5).

Despite all measures taken, the illumination is never perfectly homogeneous. To compensate in post-processing, a set of reflectance white cards is placed in the scene around the object. The distance between the object and the camera has to be the same as the distance between the cards and the camera, which means that the surfaces of these cards should lie in the same plane defined by the object. At least one card should be placed near each corner of the object so that imaginary lines connecting neighboring cards do not crop the imaged object. In our experience, fastening these cards to the easer using tape or clothes pegs that are placed on the object is a practical solution. A black background can be placed behind the object if better contrast with the white cards is required. A 99 % white reflectance standard (in our case by Labsphere (16)), a black hole (in our case by Thorlabs (17)), and a colorchecker should be placed near the imaged object. All this equipment should be visible in all

photographs and shall be within the confines of imaginary lines, connecting neighboring white cards.

A camera (in our case Nikon D850 with internal UV and IR blocking filter removed) is placed on a tripod with its lens optical axis perpendicular to the canvas and the canvas should be in the center of the camera's field of view encompassing the white cards, white standard, and the black hole. The thermometer should be placed near the imaged object too to monitor temperature and to prevent damage by overheating by illumination sources. The camera should be set to save RAW chip data with the highest bit depth possible (14 bits for our camera). We recommend disabling all proprietary image enhancement provided by the camera. For stability reasons and direct computer processing the camera is connected to a computer.

Our software package provides a very simple command line interface `cancli.py` to control the camera. It makes use of the `libgphoto2` library for Python. The program is started in terminal using command

```
python3 -i cancli.py -p,
```

where the parameter `-p` activates the camera and the parameter `-i` opens Python in an interactive mode. This program implements functions such as

```
mycam.setIso(<iso_value>),
mycam.setSpeed(<shutter_speed>),
mycam.setFnumber(<f_number>) or
mycam.focus(<focus_shift>).
```

These functions allow to set ISO, shutter speed, aperture number (typically $f/11$) and even drive the focusing motors by a precise amount of steps according to conditions as needed. Focusing is much easier and more precise with the function `mycam.previewHR()` of the `cancli.py` compared to manual focusing and using either the viewer or built-in camera display. The `mycam.previewHR()` function captures a jpeg image in full resolution and transfers it to the computer where it can be displayed on the screen. Iterating the `mycam.previewHR()` and the `mycam.focus(<focus_shift>)` allows to obtain the sharpest images.

Finally, after setting the camera, a photo is taken using `cancli.py`'s function `mycam.capture(inspect=True)`. When the image is captured, proper exposure is visualized and displayed on a computer screen. Pixels with values too close to exposure saturation (greater than 94 % of dynamic range) are depicted red while pixels in the range of 82–94 % of dynamic range are depicted green. Our software performs a direct evaluation of exposure level in the RAW file. It is, thus, independent of any white balancing. Observing the white cards as well as the white standard colored in green assures the best exposure setting providing some reasonable margin. Manual inspection instead of machine-only processing is needed because overexposed pixels corresponding to direct reflections from metallic objects (e.g. screws) are present in the image, but do not represent a problem (are not within the painting itself).

The image-capturing procedure described in previous

paragraphs is repeated twice each time with a different filter attached to the camera lens. These two filters are labeled filter A and B and were purchased from Profilocolore company (see specifications in Ref. (18; 19)). Our method is not restricted to these particular filters. It can operate with any two filters with complementary transmittances in the entire range from 300 nm to 1000 nm.

3. IMAGE PROCESSING

For better readability, all processing steps described in the following text are also depicted in a diagram in Fig 2.

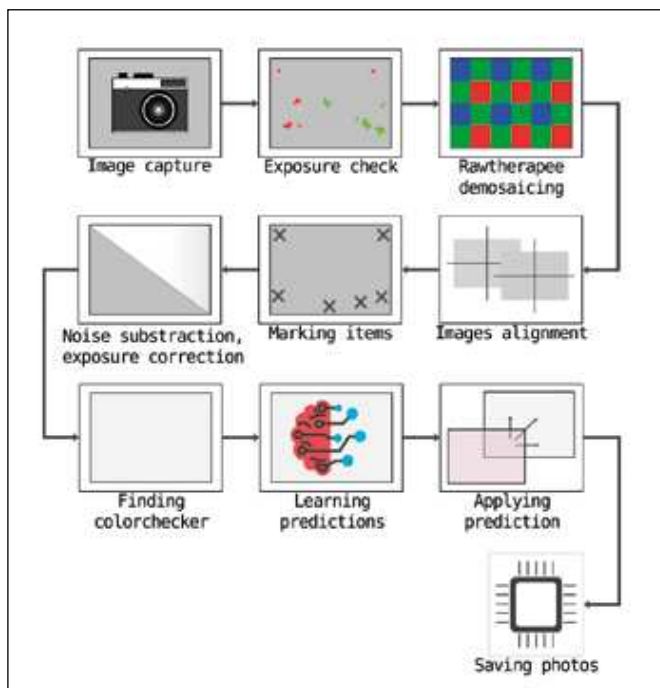


Figure 2: Image processing diagram depicting all steps as described in the text.

A Bayer mask (RGB color filters) is used in digital image sensors so that each pixel is filtered to record with different spectral sensitivity. Raw data from the sensor need to be converted from a RAW file format into RGB coordinates. A demosaicing algorithm is used to interpolate RGB values for each pixel. In our workflow, we use a free software called Rawtherapee¹. Rawtherapee is set to perform only the following image processing tasks: expected electronic noise level subtraction, demosaicing, approximative white balancing (multiplication coefficients for RGB values all close to 1), and saving RGB data with Adobe RGB profile in a 16-bit TIFF file. For exact implementation, consult Rawtherapee website.

While changing filters, we may accidentally move the camera even without noticing so the same pixel coordinates in particular photos do not correspond to each other. That is why image registration (alignment) has to be done. To align overlapping images we use Hugin² (free software) package command-line tool called `align_image_stack` with command

```
align_image_stack -a reg_ -v -m -i
-use-given-order <image_file_names>
```

where `-a` causes the output images to be saved with `reg_` prefix, `-v` (means verbose) prints progress messages, `-m` optimizes field of view for all images, except for first, `-i` optimizes image center shift for all images, except for first and using `-use-given-order` the image order as given on the command line is preserved.

The subsequent step serves to subtract sensor noise (more exact noise subtraction), stretch contrast, and compensate for non-homogeneous illumination (flat field estimation). Points of interest in the image containing the white cards, white 99 % reflectance standards, and the black hole are manually marked, using the script

```
python3 markItems.py <image_file_name>
```

This process opens a preview on display and one can move a mouse cursor to the required area and press a hotkey to mark the point. The hotkeys are `b` to mark 94 % reflectance white cards, `y` to mark the black hole and `m` to mark 99 % white reflectance standard. Upon closing the `markItems.py`, the program saves the coordinates of these points of interest into an extra file. Next, images are processed using a program `processTiff.py`, which is started using command

```
python3 processTiff.py <image_file_name> -H -i
-w.
```

Command line arguments above perform the following operations: black hole subtraction (`-H`); flat-field interpolation based on the estimation of the illumination intensity using white cards (`-i`); exposure setting so that white reflectance standard has the right RGB value (`-w`). The `processTiff.py` program outputs images using Adobe RGB color space.

Using our program `findColorchecker.py`, started through command

```
python3 findColorChecker.py
<list_of_image_file_names>
```

the colorchecker is machine detected in each image. The program also returns RGB values of each patch and saves it into a data file `colorchecker_output.dat` (when there are more photos containing colorchecker, the RGB values are written in extra columns).

Multispectral processing requires images taken using filters A and B. Our program `processMultispectral.py` is started through the command line similarly to previous programs

```
python3 processMultispectral.py
<list_of_image_file_names>
```

The industry standard by Profilocolore defines the Hyperspectral Matching Functions $HMF_i(\lambda)$, where $i \in (1, 7)$

¹<https://www.rawtherapee.com/>

²<https://sourceforge.net/p/hugin/hugin/ci/default/tree/>

(20). Given any point spectral reflectivity $R(\lambda)$, the hyperspectral values HV_i can be calculated

$$HV_i = \sum_{\lambda=300 \text{ nm}}^{1000 \text{ nm}} R(\lambda) \cdot HMF_i(\lambda). \quad (1)$$

For all the patches of our colorchecker, the hyperspectral values were obtained by direct spectroscopic measurement of reflectances $R(\lambda)$ and the application of Eq. (1). These values are saved into a definition file `colorchecker.ref1`. The ANN program takes the colorchecker photo data file (the measured $RGB_{A,B}$ values of the patches obtained from photos taken using filters A and B) `colorchecker_output.dat` and a colorchecker definition file `colorchecker.ref1` and trains to predict hyperspectral responses \overline{HR}_{ij} (j indexes colorchecker patches) based on the $RGB_{A,B}$ values. The \overline{HR}_{ij} are then compared to the definition HR_{ij} through a mean squared error

$$\Delta R^2 = \sum_{i,j} (\overline{HR}_{ij} - HR_{ij})^2. \quad (2)$$

The ANN is trained to minimize ΔR difference between the predicted and the expected (definition) values. Then the prediction is applied to all pixels of the actual image. The result of multispectral processing is in our case seven photos in seven spectral bands. Those are ultraviolet (UV), blue (B), green (G), red (R), and three infrared (IR - 1, 2, 3), corresponding to the seven hyperspectral matching functions.

3.1 ANN performance test

Because a small training dataset is available, a cross-validation technique (holdout method) is performed to establish how well the ANN was trained. The holdout method works out by removing part of the data set (in our case one patch of the colorchecker) and letting the rest of the data be used for training to get the predictions. The prediction is applied to the dataset, which was removed from the training and we can evaluate how the ANN training went. This is repeated several times for each patch on the colorchecker and the data set containing the differences ΔR between the predicted and the definition values are obtained. As depicted in Figure 3, the average values for each of the spectral bands do not exceed 0.05 (the maximum value for spectral band IR2 is 0.033 ± 0.003 concretely), which we deem to be a tolerable error.

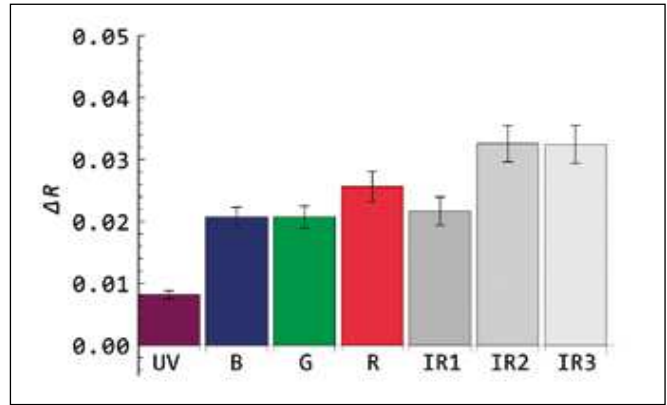


Figure 3: The average values of the cross-validation for software extrapolated multispectral imaging mode. ΔR value is depicted as a function of seven hyperspectral bands.

3.2 Ordinary visible imaging mode processing

As an additional bonus, our software package allows to estimate a colorimetrically correct photograph (in the visible part of the spectrum) of the imaged object. An image taken with the filter A³ is processed using `processColors.py` started on a command line

```
python3 processColors.py <image_file name>.
```

Similarly to multispectral processing above, the ANN makes use of the file

`colorchecker_output.dat`,
but this time with a definition data file `colorchecker.dat`.

The `colorchecker.dat` contains factory measured CIE XYZ (21) coordinates of each patch.

First of all, measured (obtained) RGB values of the colorchecker have to be converted into X, Y, Z coordinates and then (while assuming of D65 illuminant and Adobe RGB color space) into L^*, a^*, b^* coordinates. The definition data file is given in X, Y, Z coordinates, so it has to be converted into L^*, a^*, b^* as well. Then it is possible to measure the “distance” between the actual Lab coordinates and predicted Lab coordinates using Keras enabled⁴ formula for CIE color difference CIEDE2000 squared (22). The ANN is considered to be successfully trained when the average CIEDE2000 becomes comparable to the just noticeable difference value of 2.3. By cross-validation, we found the average CIEDE2000 difference to be 2.34 ± 0.27 . Then, after learning is performed and ANN is successfully trained, prediction (transformation) is applied to all pixels of the actual image. The software finally convert output (predicted) L^*, a^*, b^* coordinates through X, Y, Z back to the required Adobe RGB values. Adobe RGB 1998 profile is inserted into the output tiff file using `ImageMagick`. The result of the color processing is a colorimetrically correct photograph of the imaged object.

4. CASE STUDY

In this section, we present the results of our workflow on one selected painting. In our case, the painting has enti-

³The image should undergo the same preprocessing steps as described above: from demosaicing to automated colorchecker finding.

⁴Keras enabled means that the formula can be calculated efficiently on a graphics card.

tled The death of Sophonisba and is made by an unknown artist. Being the property of the archbishops of Olomouc, it was photographed at the Archbishop's Chateau Kroměříž.

By completely adhering procedure described in this paper we obtained seven multispectral images presented in Figure 4 and a colorimetric accurate photograph depicted in Figure 5.

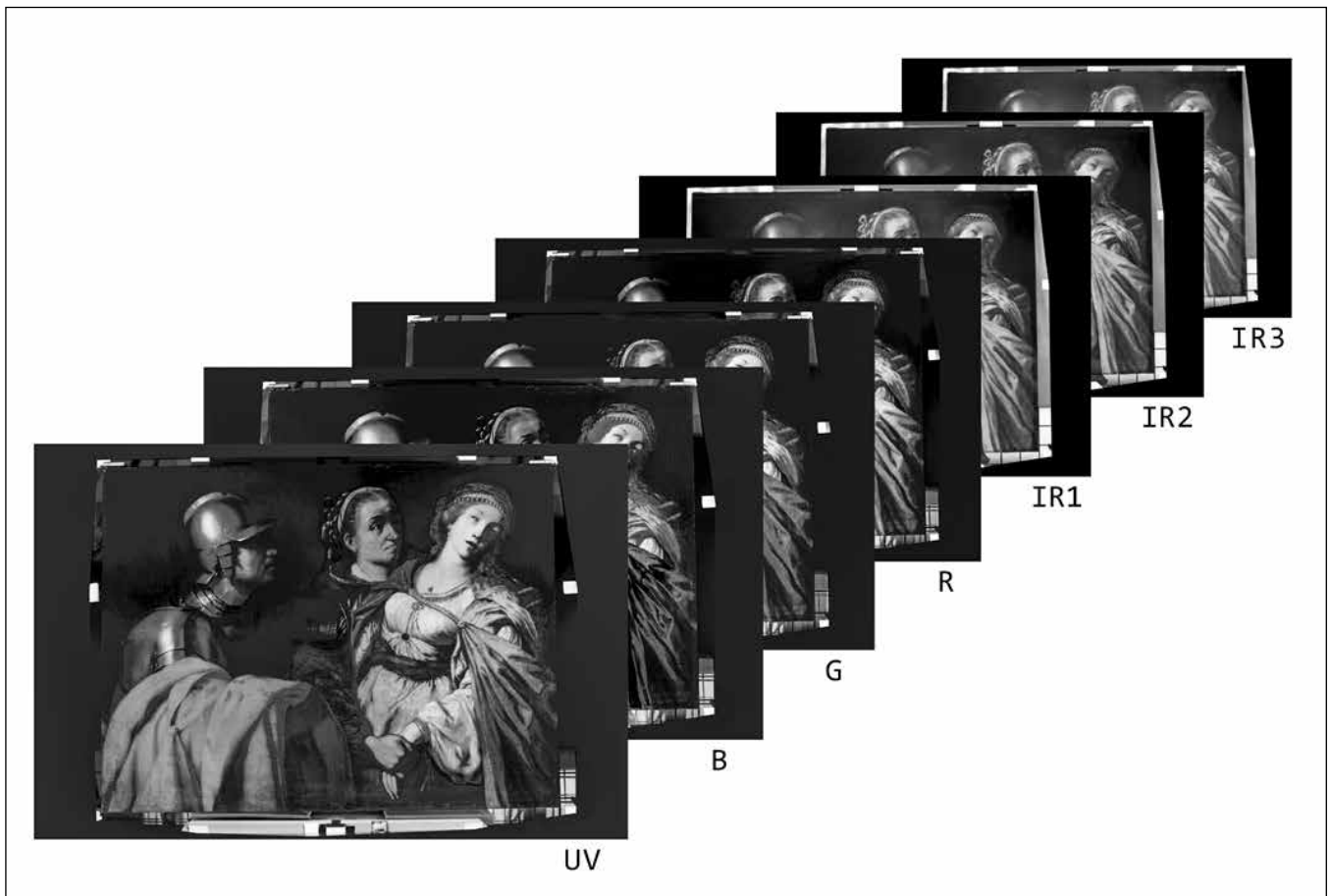


Figure 4: Result of software extrapolated multispectral imaging mode processing – multispectral images in the range from UV to IR.



Figure 5: Result of ordinary visible imaging mode processing.

5. CONCLUSION

In this paper, we have described a meticulous workflow for multispectral imaging. Our workflow is fully based

solely on open-source software including the specialized program that we distribute under a general public license. Although we have used some specific hardware components (e.g. camera, filters, colorchecker), the presented workflow does not rely on our particular choice.

To assess the quality of our procedure we have subjected the results to testing by a cross-validation method. We have found that in the case of multispectral imaging the maximum deviation between spectroscopically measured and ANN estimated hyperspectral value averaged over the entire training set was less than 5 %. This biggest deviation was found for the sixth hyperspectral band (around 850 nm). Colorimetric accuracy reaches CIEDE2000 difference of 2.34 ± 0.27 close to just noticeable difference..

On the other hand, we have registered several limitations of this method. Namely, filter B transmits the UV and IR part of the electromagnetic spectrum at the same time and the ratios of RGB values in portions of these regions are similar, so one can object, that it is not clear

which part of the spectrum caused the detection event. We thus believe that the estimation may be ambiguous, unstable or noisy. There may be a remedy to this issue by a designed different set of filters. Such analysis, however, goes beyond the scope of this paper. Further to that, it is usually difficult to sharply focus in UV and IR bands simultaneously at least with our lens. A third problem arises from the fact that the amount of detection events corresponding to IR radiation around 950 nm and UV radiation around 300 nm is comparable to noise level (while simultaneously preventing overexposure in the entire captured spectral range). This issue can be dealt with again by designing a different set of filters. Despite these limitations, we still believe that our method is conceptually valid and can serve as an invaluable tool in the analysis of cultural heritage.

ACKNOWLEDGEMENT

The authors thank CESNET for data management services.

FUNDING

This research was supported by ERDF/ESF “Arteca: Advanced physical-chemical methods of research and protection of cultural and artistic heritage”, No. CZ.02.1.01/0.0/0.0/17_048/0007378.

REFERENCES

- [1] Xun Cao. *Hyperspectral/Multispectral Imaging*, pages 1–7. 01 2021. http://dx.doi.org/10.1007/978-3-030-03243-2_841-1.
- [2] George Themelis, Jung Sun Yoo, and Vasilis Ntzichristos. Multispectral imaging using multiple-bandpass filters. *Opt. Lett.*, 33(9):1023–1025, May 2008. <http://dx.doi.org/10.1364/OL.33.001023>.
- [3] G Agresti, P Burrascano, G Calabró, C Colantonio, L Lanteri, S Laureti, M Melis, C Pelosi, M Ricci, and S Sfarra. Hypercolorimetric multispectral imaging and pulse compression thermography as innovative combined techniques for painting investigation: the case of a detached wall painting by pastura. *IOP Conference Series: Materials Science and Engineering*, 949, Nov 2020. <http://dx.doi.org/10.1088/1757-899x/949/1/012008>.
- [4] R.W.G. Hunt and M. Pointer. Measuring colour: Fourth edition. *Measuring Colour: Fourth Edition*, 07 2011. <http://dx.doi.org/10.1002/9781119975595>.
- [5] Susana Del Pozo, Pablo Rodríguez-González, Luis Sánchez-Aparicio, A. Muñoz-Nieto, David Hernandez, Beatriz Felipe, and Diego González-Aguilera. Multispectral imaging in cultural heritage conservation. *ISPRS - International Archives of the Photogrammetry, Remote Sensing and Spatial Information Sciences*, XLII-2/W5:155–62, 08 2017. <http://dx.doi.org/10.5194/isprs-archives-XLII-2-W5-155-2017>.
- [6] Cerys Jones, Christina Duffy, Adam Gibson, and Melissa Terras. Understanding multispectral imaging of cultural heritage: Determining best practice in msi analysis of historical artefacts. *Journal of Cultural Heritage*, 45:339–350, 2020. <http://dx.doi.org/10.1016/j.culher.2020.03.004>. URL: <https://www.sciencedirect.com/science/article/pii/S1296207419308064>.
- [7] Antonino Cosentino. Multispectral imaging and the art expert. *Spectroscopy Europe*, 27, 01 2015.
- [8] James Robinson, Eileen Frame, and George Frame. *Introduction to Spectroscopy*, pages 61–100. 05 2021. <http://dx.doi.org/10.1201/b21879-2>.
- [9] Barbara Berrie. Rethinking the history of artists’ pigments through chemical analysis. *Annual review of analytical chemistry (Palo Alto, Calif.)*, 5:441–59, 07 2012. <http://dx.doi.org/10.1146/annurev-anchem-062011-143039>.
- [10] Rijksmuseum. The initial results of operation night watch, 2020. URL: <https://www.rijksmuseum.nl/en/the-initial-results-of-operation-night-watch>.
- [11] Antonino Cosentino. Identification of pigments by multispectral imaging: A flowchart method. *Heritage Science*, 2:12, 04 2014. <http://dx.doi.org/10.1186/2050-7445-2-8>.
- [12] Joanne Dyer, Giovanni Verri, and John Cupitt. *Multispectral Imaging in Reflectance and Photo-induced Luminescence modes: A User Manual*. 10 2013.
- [13] Anna Pelagotti, Andrea Del Mastio, Alessia De Rosa, and Alessandro Piva. Multispectral imaging of paintings. *Signal Processing Magazine, IEEE*, 25:27–36, 08 2008. <http://dx.doi.org/10.1109/MSP.2008.923095>.
- [14] Digital supplement containing software sources available from publisher’s website.
- [15] Jan Gooch. *Color Rendering Index*, pages 157–157. 01 2011. http://dx.doi.org/10.1007/978-1-4419-6247-8_2663.
- [16] Labsphere. Spectralon diffuse reflectance targets, 2020. SRT-99-020. URL: https://www.artisantg.com/info/Labsphere\SRT\99\120_Datasheet\201591892113.pdf.
- [17] Thorlabs. Beam trap, 2013. BT600. URL: <https://www.thorlabs.com/drawings/\2785d435c48c70aa-FEA80DF1-9138-62E9-9671F1A50D91F8A7BT600\M-SpecSheet.pdf>.
- [18] Profilocolore. Measurement report - transmission, 2021. URL: https://www.profilocolore.com/wp-content/uploads/2021/05/PFCL-A_77x2.pdf.
- [19] Profilocolore. Measurement report - transmission, 2021. URL: https://www.profilocolore.com/wp-content/uploads/2021/05/PFCL-B_77x2.pdf.

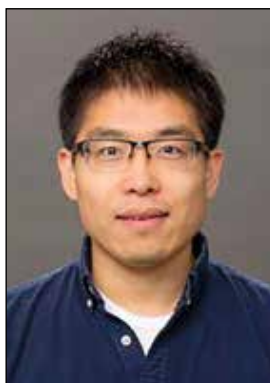
- [20] Marcello Melis, Matteo Miccoli, and Donato Quarta. Multispectral hypercolorimetry and automatic guided pigment identification: some masterpieces case studies. In Luca Pezzati and Piotr Targowski, editors, *Optics for Arts, Architecture, and Archaeology IV*, volume 8790, pages 208–221. International Society for Optics and Photonics, SPIE, 2013. <http://dx.doi.org/10.1117/12.2020643>.
- [21] D. Rowlands. *CIE XYZ Color Space*. 04 2020. <http://dx.doi.org/10.1117/3.2542355.ch55>.
- [22] Ming Luo, Guihua Cui, and B. Rigg. The development of the cie 2000 colour difference formula: Ciede2000. *Color Research & Application*, 26:340–350, 10 2001. <http://dx.doi.org/10.1002/col.1049>.

Daniela Růžičková (daniela.ruzickova02@upol.cz), Bc. Jindřich Švihel (jindrich.svihel@upol.cz), Mgr. Antonín Černoch, Ph.D. (antonin.cernoch@upol.cz), doc. Mgr. Karel Lemr, Ph.D. (k.lemr@upol.cz) Palacký University in Olomouc, Faculty of Science, Joint Laboratory of Optics of Palacký University and Institute of Physics of the Czech Academy of Sciences, 17. listopadu 50A, 772 07 Olomouc, Czech Republic

Jedná se o vědecký článek

Cena ICO za topologickou fotoniku

Po Čen (Bo Zhen) z Katedry fyziky a astronomie na Pensylvánské univerzitě (USA) byl vyznamenán cenou ICO 2020 (ICO – *International Commission for Optics*) za „průkopnictví v oblasti výzkumu a vývoje optických vázaných stavů v kontinuu (optical bound states in the continuum), výjimečných bodů (exceptional points) a dalších topologických stavů ve fotonice“. Prof. Po Čen získal titul B.S. z matematiky a fyziky na čínské Univerzitě Čching-chua a doktorát z fyziky na americkém Massachusettském technologickém institutu. Jeho skupina na Pensylvánské univerzitě se zaměřuje na nové jevy v topologických fotonických systémech a jejich aplikace v nelineární optice, optoelektronice a kvantové elektronice. Tato cena byla udělena na základě jeho příspěvků k objevům a pochopení topologických stavů ve fotonice, které zahrnují topologickou povahu optických vázaných stavů v kontinuu [1, 2], kruhy bodů narušujících PT (parity-time) symetrii (exceptional rings) [3] a objemové Fermiho oblouky (bulk Fermi arcs) [4] v optických systémech a jednosměrně vedených rezonancích (unidirectional guided resonances) [5]. V poslední době jeho skupina na Pensylvánské univerzitě rozšířila výzkum topologické fotoniky za hranice lineárních struktur na obecné nelineární optické systémy. Ve své práci identifikovali řadu nových topologických fází, které neexistují ve statických systémech, ale objevují se, když je systém periodicky napájen vnějším polem. Mezi příklady patří Floquetovy-Chernovy izolátory světla [6] a Floquetovy dipólové fáze (Floquet



dipole phases) [7]. Navrhli také metodu, jak výrazně potlačit nebo dokonce zakázat nežádoucí generování nelineárních frekvencí pomocí topologických metod [8]. Tyto výsledky otevírají cestu k budoucímu zkoumání a klasifikaci všech možných topologických fází v řízených nelineárních optických systémech. Tyto vědecké poznatky najdou uplatnění v optoelektronice a mohou vést k novým funkcím významně překonávajícím stávající přístupy.

Literatura

- [1] *Physical Review Letters* 113, 257401 (2014).
- [2] *Nature* 499 (7457), 188–191 (2013).
- [3] *Nature* 525 (7569), 354–358 (2015).
- [4] *Science* 359 (6379), 1009–1012 (2018).
- [5] *Nature* 580 (7804), 467–471 (2020).
- [6] *Nature Communications* 10, 4194 (2019).
- [7] *Physical Review Letters* 126, 113901(2021).
- [8] *Nanophotonics* 10 (17), 4233–4239 (2021).

*Prof. Leszek Sirko, viceprezident ICO, předseda Výboru pro udělování cen ICO
ICO Newsletter leden 2022*